ORIGINAL PAPER

Comparison of Cycling High Temperature Corrosion at 650°C in the Presence of NaCl of Various Austenitic Stainless Steels

Mirjam Bajt Leban[1] · Maja Vončina[2] · Tadeja Kosec[1] · Robert Tisu[3] · Matevž Barborič[2] · Jožef Medved[2]

Abstract

The high temperature corrosion at 650°C in the presence of NaCl at atmospheric pressure of AISI 304L, AISI 309, AISI 310S, AISI 314 and AISI 321 austenitic stainless steel was studied. The specimens were cyclically heated in the furnace and immersed in a 3.5% aqueous NaCl solution after cooling for 15 min. After each cycle, the change in mass of the samples was measured. The corroded samples were analysed by SEM /EDX, and the corrosion products were analysed by XRD. The chloride ions react with the steel surface to form porous and poorly adherent oxides and metal chlorides. After the mass increase during the first exposure cycles, spalling of the oxides occurred. The high temperature austenitic stainless steels (AISI 309, AISI 310S, AISI 314) showed less mass loss than conventional austenitic steels (AISI 304L). Surprisingly, the stainless steel AISI 321 showed a similar low weight loss after the cyclic test as AISI 309, but a detailed analysis of the exposed surfaces after the test showed a similar corrosion attack as for AISI 304. After the cyclic test at high temperature in the presence of NaCl, a higher concentration of Cr and Ni definitely improves the corrosion resistance under the present conditions, but a certain addition of Si is even more obvious.


✉ Mirjam Bajt Leban
    mirjam.leban@zag.si

1   Slovenian National Building and Civil Engineering Institute, Dimičeva 12, 1000 Ljubljana, Slovenia

2   Faculty of Natural Sciences and Engineering, Department of Materials and Metallurgy, University of Ljubljana, Aškerčeva Cesta 12, 1000 Ljubljana, Slovenia

3   Akrapovič d.d, Malo Hudo 8a, 1295 Ivančna Gorica, Slovenia

Graphical Abstract
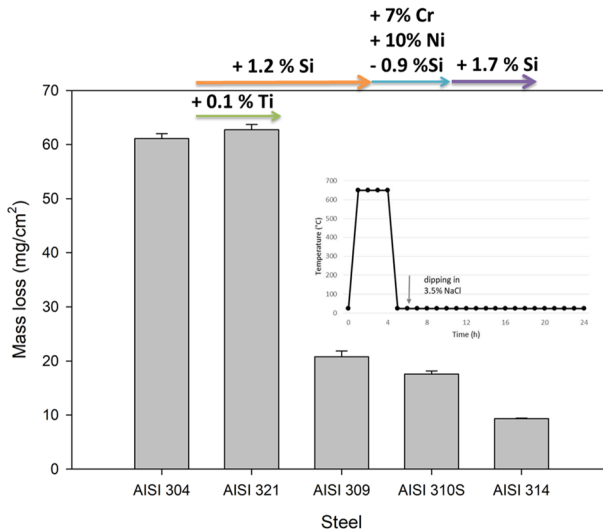
Introduction

Austenitic stainless steels are used in various applications due to their excellent corrosion resistance in many corrosive environments, including high chloride concentrations under atmospheric conditions. One of not often studied areas is automotive exhaust systems, which operate at high temperatures with peaks of up to 1000°C near the engine [1]. In addition to high temperatures, the presence of salts from winter road de-icing accelerates the corrosion of exhaust components and leads to their degradation [2]. In recent decades, stainless steels have partially replaced low alloy steels in exhaust systems due to their longer life and better appearance [3]. Some parts of exhaust systems, such as the dampers, are intentionally made of steels that are more resistant to harsh conditions because they can function reliably even in an unfriendly environment. However, the price and reliability of the final product are very important in the automotive industry, so it is always necessary to consider all options and choose the most optimal.

Several so-called high-temperature austenite steels are known for their oxidation resistance and satisfactory mechanical properties at high temperatures. Excellent corrosion resistance in a harsh environment at room temperature or slightly elevated temperature, as well as oxidation resistance at high temperatures, is due to the formation of a chromium oxide layer in an oxidative atmosphere [4]. During exposure to air (atmospheric conditions) a protective chromium oxide is formed. During

exposure at higher temperatures, this oxide changes. At moderate temperatures, the oxide becomes even more protective due to the slow diffusion of oxygen through the oxide. However, when temperatures rise and a corrosive environment, for example NaCl, KCl or other salts are present, the chromium oxide is no longer protective. Cao et al. [5] reported that while the mass gain during 20 h long exposure at 600°C remain almost zero, in the presence of NaCl it was approximately 7 mg/cm^2. In addition, the difference between the coefficients of linear thermal expansion of oxides and metals causes the voluminous oxides to flake off when temperatures change [6]. Corrosion and even oxidation at high temperatures act in two directions: it forms scale at the surface and changes the elemental composition in the subsurface of an alloy [7]. Chromium is not the best alloying element to improve the corrosion resistance of steels in the presence of NaCl, either as solid deposit, or sprayed to the surface. Chromium has been found to accelerate corrosion rate and penetration below the melting temperature of NaCl (which is 801°C) [8, 9] via oxychlorination of Cr-oxide and formation of Na_2CrO_4. Thus, NaCl/ Na_2CrO_4 eutectic system with melting point 577°C is present, which increase corrosion rate of stainless steels significantly [5, 10, 11]. Ni reaction with NaCl and oxygen at temperatures around 600 °C is not very probable; therefore, ferritic stainless steels are more susceptible to corrosion than austenitic stainless steels [10, 12]. The main reason for this behaviour is the higher concentration of Ni in austenitic grades. The mass loss due to corrosion under such conditions increases with Cr content and decreases with Ni content in the alloy [13]. In several studies, it has been shown by combined metallographic and SEM observation of the material cross section that the subsurface layer becomes porous and depleted in chromium and iron but enriched in nickel under such conditions [14]. Therefore, nickel-based alloys are much more resistant than stainless steels at high temperatures in the presence of chlorides [2, 13, 15–20].

There are two strategies for improving the high temperature resistance of stainless steels: increasing the chromium and nickel content or adding silicon, nitrogen and rare earths. When the critical concentration of chromium is reached, a less protective iron oxide forms instead of chromium oxide. Chromium and nickel improve the oxidation/corrosion behaviour at higher temperatures, but on the other hand increase the occurrence of brittle phases such as the sigma phase. The addition of nickel improves creep and spalling resistance (improves adhesion of scale to alloy) at temperature cycling and increases corrosion resistance in various environments. The addition of cerium (rare earth element) in combination with silicone improves oxidation stability, resistance to erosion corrosion and reduces oxide spalling. Silicone is added to the alloy to form an underlayer that provides a diffusion barrier for iron. The weak point of high temperature stainless steels is the development of the sigma phase at temperature changes between 600 and 900°C, which reduces the ductility and elongation of the alloy at room temperature. The development of the sigma phase can be successfully retarded by the addition of carbon and nitrogen [21]. Low silicon addition has been shown to reduce the oxidation rate of ferritic Fe–Cr and austenitic Fe–Cr-Ni steels by forming a very thin Si fayalite layer between chromium scale on the surface of the alloy and the alloy—such a Si layer provides a barrier to chromium transport from the alloy to the surface [1, 6, 9, 19–24]. Chromium and silicon in the oxide layer are concentrated near the steel and

form $FeCr_2O_4$ and Fe_2SiO_4. In the initial phase of oxidation, oxides are first formed: SiO_2, Cr_2O_3, Fe_2O_3, Fe_3O_4 and FeO. After some time of oxidation, Cr_2O_3 and SiO_2 are surrounded by FeO and finally $FeCr_2O_4$ and Fe_2SiO_4 oxides are formed [25]. Buscail and others [26, 27] studied the effect of molybdenum on the oxidation of stainless steel at 900°C and 1000°C and found that molybdenum affects oxidation similarly to silicon. However, the role of silicon added in stainless steels at high temperature in the simultaneous presence of NaCl is not fully understood [10, 28].

However, only a small amount of chloride in the atmosphere at high temperatures causes stainless steel corrosion resistance to be completely lost [29]. During cooling from higher temperatures, hydrochloric acid may be formed from chlorine by reaction with hydrogen or water vapour. Under these conditions, the protective chromium oxide is degraded, and less stable metal spinels and hydroxides are formed. In addition, easily vaporizable metal chlorides can be formed. Since the partial vapour pressure of metal chlorides is lower than that of metal oxides, they evaporate at lower temperatures than oxides. This phenomenon is observed not only in the presence of chlorides, but also in the presence of all other halide ions. The corrosion rate of Fe–Cr stainless steels in the presence of chlorides at temperatures above 500°C depends on the sublimation of iron and chromium chlorides. Below this temperature, the corrosion rate decreases with the chromium content in the alloy and the oxygen content in the atmosphere [16, 22, 30–32].

Above 500°C, the depth of penetration of corrosion increases dramatically in the presence of chlorides. The depth of penetration of internal corrosion increases with carbon content. On the other hand, under these conditions, silicone and molybdenum improve general and intergranular corrosion [9]. Protective oxide layers are usually a mixture of a solid solution of iron and chromium oxide. Oxides with a larger Cr/Fe ratio are protective. Processes that cause a reduction of chromium in the oxides are detrimental and lead to an enrichment of the oxide with less protective iron [33].

The aim of this research was to study the high temperature corrosion degradation of austenitic stainless steel under condition simulating corrosion of external exhaust surfaces used during winter condition. The influence and the role of alloying elements Cr, Ni and Si at tested condition are discussed.

In this study five different austenitic stainless steels (AISI 304L, AISI 321, AISI 309, AISI 310S and AISI 314) were exposed to combined action of chloride ions at elevated temperatures in order to compare their high temperature resistance under so harsh condition. At the end of each cycle, the change in mass of the samples was measured. After the end of exposure, the corroded samples were analysed by SEM/EDX, and the corrosion products were analysed by XRD.

Experimental Procedures

Samples of six types of stainless steel (AISI 304L, AISI 321, AISI 309, AISI 310S, and AISI 314; the chemical analyses from the technical sheets are listed in Table 1) were cut in the form of cylinders of 10 mm diameter and 20 mm length. Before exposure, all specimens were manually ground with 320 grit SiC abrasive paper and ultrasonically cleaned in acetone.

Table 1 Standard and cast analysis chemical composition (in weight %) of tested materials

	Fe	Cr	Ni	Mn	Si	C	P	S	Mo	Ti	N
AISI 304L-1.4306, 1.4307 (standard)	rest	17.5–19.5	8.0–10.5	<2.0	<1.0	<0.03	<0.045	<0.015	/	/	<0.10
AISI 304L-1.4306, 1.4307 (cast analysis)	rest	18.195	8.01	1.453	0.318	0.026	0.021	0.025	0.3	/	0.091
AISI 321 -1.4541 (standard)	rest	17.0–19.0	9.0–12.0	<2.0	<1.0	<0.08	<0.045	<0.015	/	5xC to 0.70	/
AISI 321 -1.4541 (cast analysis)	rest	17.09	9.31	1.63	0.36	0.0312	0.0503	0.0197	0.282	0.463	0.0145
AISI 309-1.4828 (standard)	rest	19.0–21.0	11.0–13.0	<2.0	1.5–2.5	<0.2	<0.045	<0.015	/	/	/
AISI 309-1.4828 (cast analysis)	rest	19.09	11.285	1.543	1.8	0.056	0.0291	0.0015	0.296	/	0.047
AISI 310S -1.4845 (standard)	rest	24.0–26.0	19.0–22.0	<2.0	0–1.5	<0.10	<0.045	<0.015	/	/	/
AISI 310S -1.4845 (cast analysis)	rest	24.74	19.41	1.14	0.73	0.044	0.031	0.001	/	/	0.059
AISI 314 -1.4841 (standard)	rest	24.0–26.0	19.0–22.0	<2.0	1.5–2.5	<0.2	<0.045	<0.015	/	/	/
AISI 314 - 1.4841 (cast analysis)	rest	24.2	19.16	1.64	2.25	0.025	0.023	<0.001	/	/	0.02

The samples were subjected to cyclic oxidation. A typical cycle (Fig. 1) consisted of exposure in the furnace at 650°C at atmospheric condition for 4 h. After exposure in the furnace, the samples were taken out from the furnace, cooled to room temperature (23 ± 2°C, 50 ± 5%RH). One hour after the samples cooled down to room temperature, they were fully immersed in a 3.5% NaCl aqueous solution for 15 min. Then, the samples were held at laboratory conditions until the cycle was completed at 24 h. A total of five cycles were performed. Before the first cycle and after each cycle, all samples were weighed. After the fifth weighing cycle, the corrosion products of the samples were carefully removed and collected for XRD analysis. Then, the samples were cleaned in a 50% aqueous HCl solution with the addition of a corrosion inhibitor to completely remove the oxide film. Afterwards, all samples were weighed. Mass gain (after each cycle of exposure) and mass loss (after descaling at the end of fifth cycle) are given as mg/cm^2.

After completion of the exposure, a sample cross section of each type of steel was cast in cold epoxy, grinded in the presence of water with 320 SiC abrasive paper and polished with 9 μm and 3 μm diamond suspension (MetaDi Supreme, Poly) and finally with 0.05 μm alumina polishing suspension was used in order to observe the morphology and analyse the elemental composition of the corrosion products.

Metallographic examination of the surface oxide layer was carried out with Zeiss Imager.Z2m using AxioVision 4.6 software. The corrosion layers of the same samples were examined using JEOL JSM-IT500LV scanning electron microscope. Energy-dispersive X-ray (EDX) analyses were performed using Oxford software AZtec to study the morphology and composition of the scales. For XRD analysis, the corrosion products were mechanically removed from the samples after the 5th exposure cycle and placed in a Zerro backplate holder while they were analysed using PANalytical Empyrean. XRD spectra were recorded between °2θ angles 5.2 and 100°. The step size was 0.01313°, and the time per step was 119.85 ms. The XRD data were analysed using HighScore Plus database software.
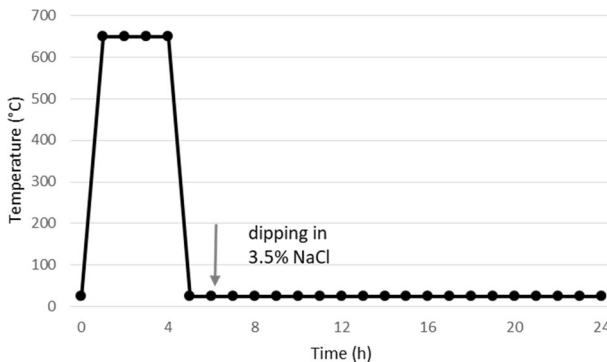
Fig. 1 Typical cycle of sample exposure, five cycles performed in the study

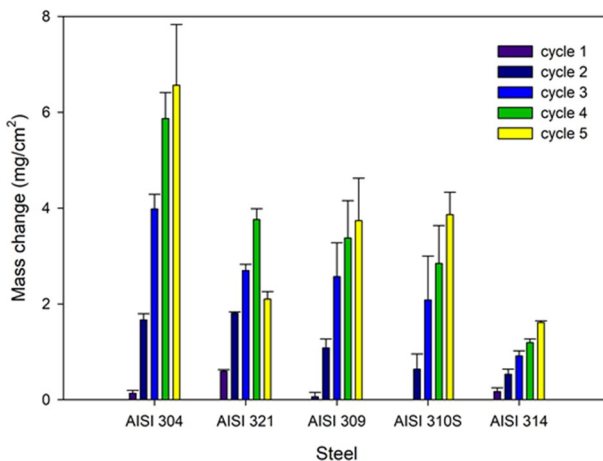## Results

Corrosion Kinetics

The rate of mass gain/loss for the austenitic stainless steels tested at 650°C in the presence of NaCl after each exposure cycle is shown in Fig. 2. All materials tested show an average increase in mass throughout the exposure period (all five cycles). The lowest mass increase over the tested period was measured for the AISI 314 and the highest for the AISI 304L stainless steel. The mass increase for the AISI 309, AISI 310S and AISI 321 steels is comparable. However, for the AISI 321 stainless steel, a mass loss was observed in the fifth cycle. The stainless steel AISI 314 shows the smallest mass increase, while the standard deviations for each cycle are the smallest.

Figure 3 shows the data of the weight of the samples after the gentle mechanical and chemical removal of the scale at the end of the temperature cycling. It can be seen that by far the largest mass loss occurs for AISI 304L steel and AISI 321, which is between 60 and 65 mg/cm^2, followed by AISI 309 and AISI310S (around 20 mg/cm^2). The mass loss for AISI 314 stainless steel was the least among the materials studied, approximately 10 mg/cm^2.
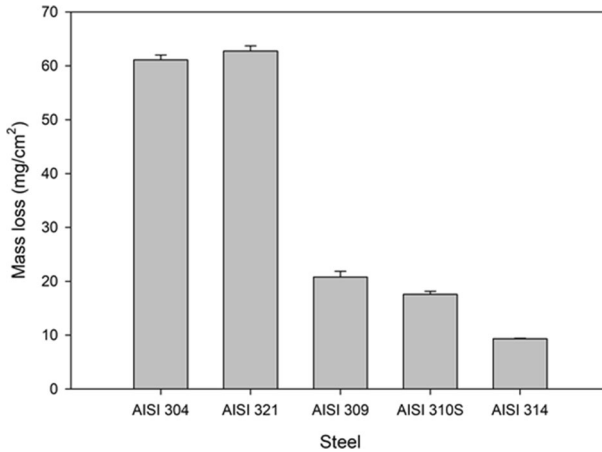
Scale Structure and Composition of Corrosion Products

SEM/EDS Analysis

Typical corrosion scales and the EDS analysis of the main chemical elements (Fe, Cr, Ni, Mn, Si, O and Cl) in the alloys to understand the corrosion behaviour

Fig. 2 Results of mass change after each cycle of exposure at 650°C in the presence of NaCl (no scale removal performed)

Fig. 3 Results of mass loss after the end of five cycles of exposure at 650°C in the presence of NaCl (after scale removal)

under the studied conditions are shown in Fig. 4. It can be observed that the corrosion products of AISI 304 and AISI 321 steels are much more voluminous than the corrosion products of the other three steels. The thickness of the corrosion product layer on AISI 309 and AISI 314 is less than that on the surface of AISI 310.

As shown in Figures SEM and EDX, the corrosion products of AISI 304L and AISI 321 are multilayered (Fig. 5a and b, respectively), with the layers separated and differing in chemistry. Iron oxides or spinels with the alloying elements Cr and Mn predominate. Porosity is present in the intermediate layer between the steel and the corrosion product. The porosity of AISI 321 is finer than the porosity of AISI 304L. Within the porous region, enrichment in Ni and depletion in Cr are observed in both materials. On stainless steels AISI 309, AISI 310S and AISI 314 similar features and heavily reduced thickness of surface deposits was observed. Iron oxide is present on the upper surface of the corrosion products of AISI 310S, and the lower layer of the corrosion products consists of Fe, Cr, Mn oxide or spinel (Fig. 5d). Low porosity is observed in the intermediate layer between the corrosion products and the steel. Similar to AISI 304L and AISI 321, there is a Ni enriched zone and a Cr depleted zone in this interlayer. The morphology of the corrosion products of AISI 309 and AISI 314 (Fig. 5c and e, respectively) is similar: the layer of corrosion products is compact and thin (comparable to the corrosion products of the other steels tested) and consists of Fe, Cr and Mn oxides or spinel. In the interlayer, a zone enriched with Ni and a zone depleted with Cr can also be observed in these two steels, but no porosity and no corrosion attack on the interior, as was the case with the other three steels. The presence of Cl in corrosion products was observed only in steels AISI 304L, AISI 321 and AISI 309, which showed the highest corrosion rate, respectively. However, Cl presence was also influenced by preparation of specimens before observation by using water containing stepwise grinding which could partially dissolve Cl to some extent.
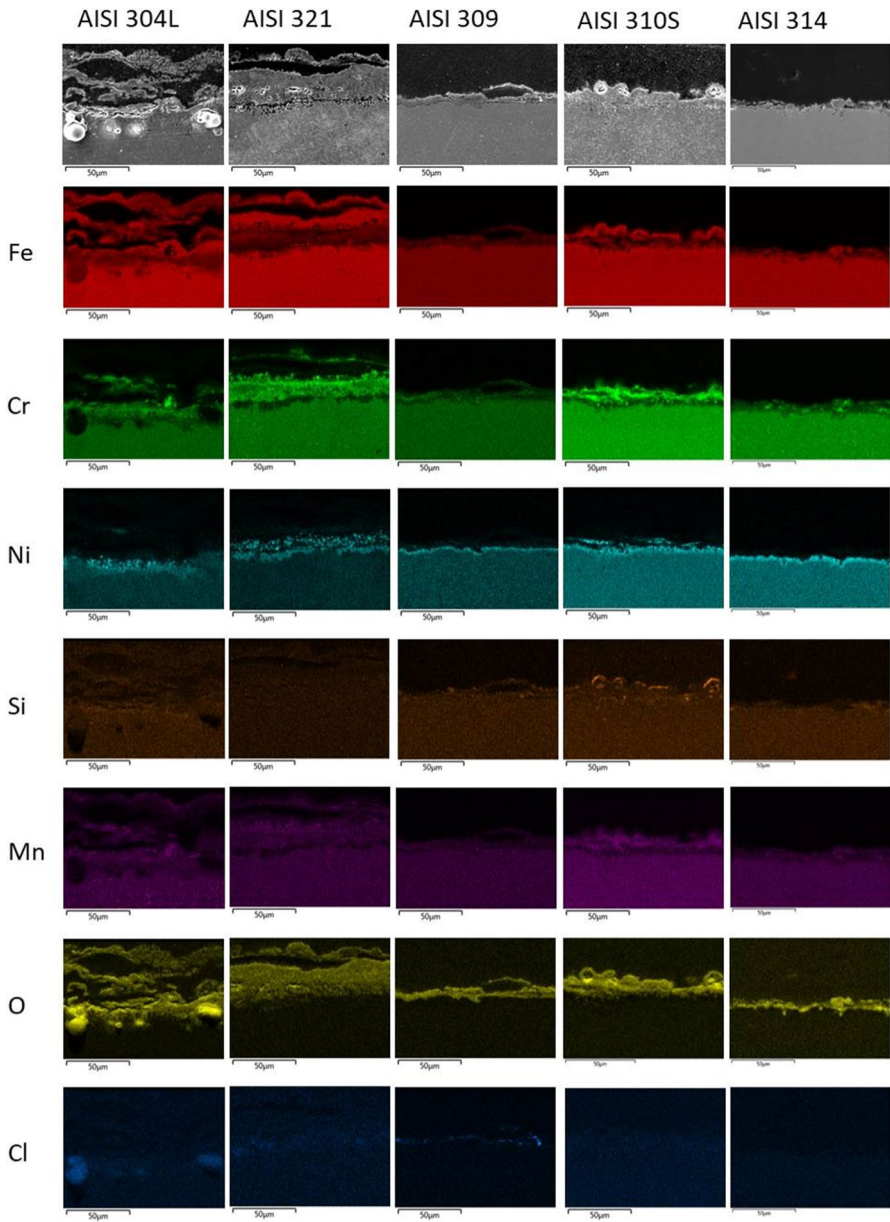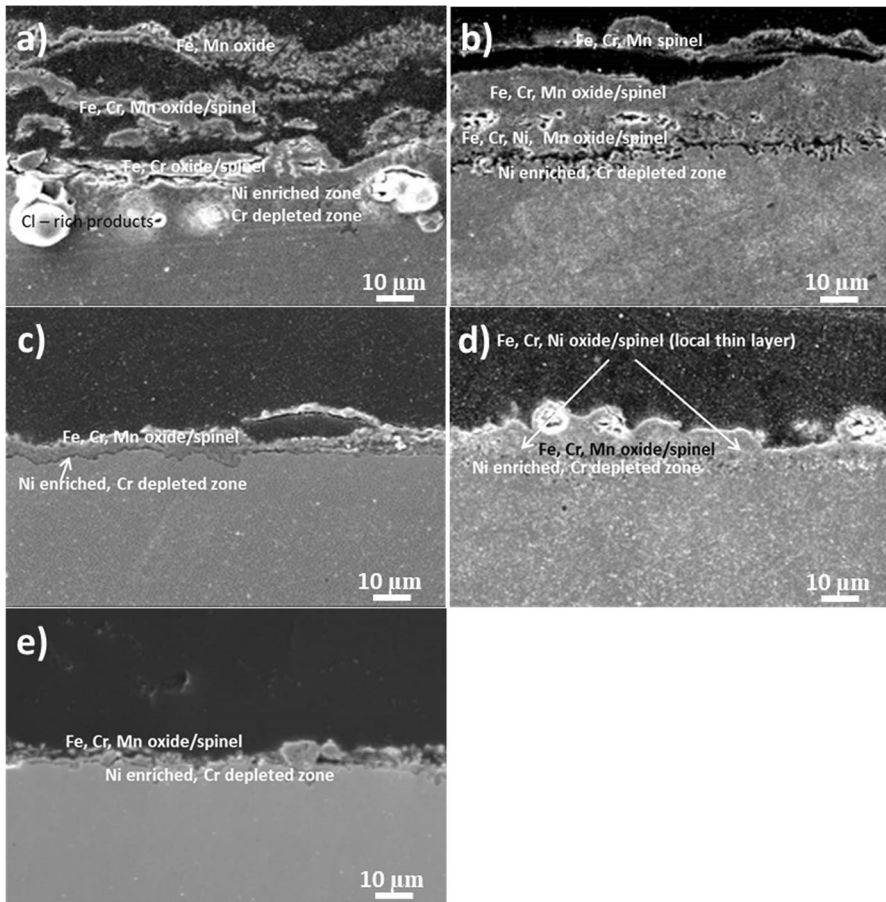
Fig. 4 SEM image and SEM/EDX elemental distribution maps of Fe, Cr, Ni, Mn, Si, O and Cl in the developed surface deposits after fifth cycle

XRD Analysis

The diffraction patterns obtained by the analysis of the corrosion products have shown that all the peaks are present in different angular positions for all the five

Fig. 5 Morphology of corrosion products in a cross-sectional view for **a** AISI 304L, **b** AISI 321, **c** AISI 309, **d** AISI 310S and **e** AISI 314

steels studied, as presented in Fig. 6. As can be seen from the elemental maps on EDS in Figs. 4 and 5a to d, the corrosion products consist mainly of Fe, Cr and Mn oxides and/or spinels [34, 35]. XRD analysis revealed the presence of Fe oxides, Cr_2O_3 and Fe, Cr and Mn spinels. In addition, NaCl was also detected. The intensity (number of counts) of the detected peaks at the same position cannot be compared, since the same amount of corrosion products was not analysed for each of the steels studied. The largest amount of corrosion products was collected (and placed in the analysis holder) for the AISI 321 steel, which has the highest intensities in Fig. 6. On the other hand, the least amount of corrosion products was analysed for the steel AISI 310S.
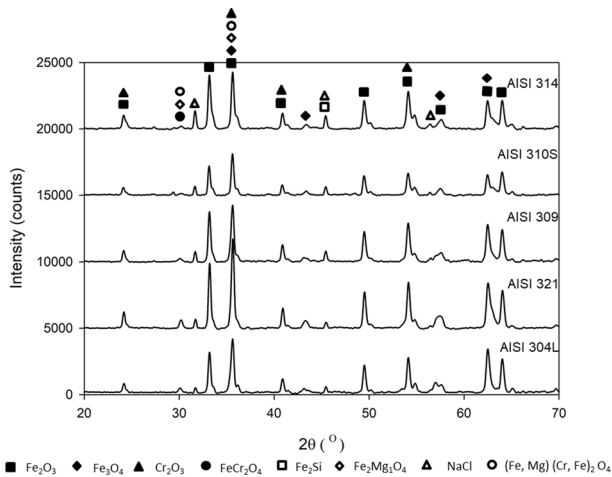
Fig. 6 XRD patterns of AISI 304L, AISI 321, AISI 309, AISI 310S and AISI 314 corrosion products formed after 5th cycle of exposure to 650 °C and immersion in NaCl

Discussion

Regardless of the type of stainless steel tested, thicker, dark-coloured scale formed at the end of the 2nd exposure cycle when the surface of the tested specimens was contacted with NaCl and then subjected to high temperature (650 °C). During the 1st cycle at furnace, specimens surfaces were covered by thin layer Cr_2O_3. In the second part of this cycle, once the Cr-oxide was already formed, short-time dipping into NaCl, after evaporating of water at laboratory condition, NaCl species remains at the surface. In the next, 2nd cycle, when heated to 650°C, NaCl reacted with Cr_2O_3 and Na_2CrO_4 and HCl are formed by this reaction, which accelerated significantly mass gain (Fig. 2). Further, HCl diffuse towards the substrate and react with Fe and Cl then forming $FeCl_2$ and $CrCl_3$ [9, 18, 30, 31, 36]. By continuing to cycle, and newly deposited NaCl by dipping to the stainless steel surface, NaCl and previously formed Na_2CrO_4 forms eutectic with melting point at 577°C, which even accelerate corrosion and formation of non-protective porous scale with low adhesive strength and its thickening from cycle to cycle [10]. Oxidation of Fe and Cr leads to weight increase by time, while oxychlorination and chlorination of the same alloying elements leads to weight loss via low adhesivity of these products and their brittleness. That can be explained by calculated Gibbs free energies for MCl_2 formation (M is metal), which are sorted in the following order from negative to more positive values: Cr < Fe < Ni. This means that under these conditions chromium and iron chlorides are formed first [18, 31]. The temperature variations during the test also led to cracking and spalling of the oxide layer, making it easier for the chloride to penetrate the underlying metal at the test temperature in the furnace. In the case of this study, both processes, oxidation, and chloride reaction, are involved and contribute to the corrosion processes on the steel surfaces. Because the oxidation products formed during exposure evaporate and spell out to some degree, the results of weight measurements are not always

a realistic indicator of the extent of corrosion. In addition, varying moisture contents on the scale can lead to an overestimation of the weight. The best way to get an overview is to perform a chemical descaling after each cycle to see how much the steel has oxidized. Unfortunately, such an approach requires testing and evaluating numerous samples. In the case of this study, descaling was only performed after the last cycle and the weight loss was then measured.

From Fig. 2, which shows the mass gain/loss after each cycle, and Fig. 3, which shows the weight loss after removing of the corrosion products at the end of the exposure, it can be seen that the highest weight loss is found for AISI 304L and AISI 321 steels. This result is consistent with the literature and with the alloying elements present in both steels. These two steels contain the lowest Cr and Ni content among the tested materials. Slightly better corrosion resistance of AISI 321 was expected compared to AISI 304L due to the better resistance to intergranular attack achieved by the addition of Ti as a carbide-bonding alloying element [37, 38], however in our study it was not observed.

In comparison to AISI 304L and AISI 321, slightly higher concentrations of Cr (1 and to 2%, respectively) and Ni (1.3 and 3.3%, respectively) in AISI 309, resulting in more than one time lower mass loss after cleaning at the end of the test. In addition to Cr and Ni, AISI 309 contains 1.5% more Si than compared steels, whose effect to improve oxidation resistance is known from the literature [4], but studies on the effect of Si on corrosion at high temperatures in the presence of chlorides are lacking. Based on the results of this study, we found that Si-containing oxide does not develop at elevated temperatures and exposure to aqueous NaCl solution. In the EDS mapping results (Fig. 4), no enrichment with Si was observed at the scale-to-alloy interface as reported in oxidation tests in air (no halide ions present) [21, 22]. On the other hand, both steels with higher Si addition (1.8% for AISI 309 and 2.25% for AISI 314) exhibit the thinnest and most compact corrosion products observed when examining the sample cross section after the end of corrosion exposure. Ni enrichment and Cr as well as Fe depletion directly below the scale-to-alloy interface is present in all the specimens studied. However, the thickness of this zone increases in the same order of magnitude as the mass gain/loss. A Ni enriched zone is present directly below the scale-to-alloy interface (on the alloy side) and a Cr enriched zone is present above the scale-to-alloy interface (on the scale side) for all the alloys investigated. The Fe content in this zone above and below the scale-alloy interface is low. However, it is very likely that Si in AISI 309 is present in sufficiently high concentrations so that provides a barrier to the diffusion of Cr into the atmosphere and its oxidation and/or chlorination, and greatly improves the adhesion of corrosion products to the steel surface. AISI 310S contains a much higher concentration of Cr and Ni than AISI 309, but a lower concentration of Si. Its corrosion behaviour at high temperatures is slightly better than that of AISI 309 showing that 1% of Si addition at present corrosion conditions is equivalent to addition of approximately 5%Cr and 8%Ni. If we compare AISI 310S and AISI 314, which have approximately the same concentration of Cr and Ni, we can see that the mass loss of AISI 314 is lower. This is again most likely the result of the higher concentration of Si, which is in AISI 314 for 1.5% higher than in AISI 310. Among the tested steels with lower Si concentration but different Cr and Ni content, we can compare AISI 304L and AISI

321 (about 18 wt% Cr and 8–9 wt% Ni) with AISI 310S, which contain about 25 wt% Cr and 19% Ni. AISI 310S, which contains almost 40% more Cr and one times more Ni than AISI 304L and AISI 321, shows much lower corrosion damage after the test; mass loss after testing and descaling is almost one times lower.

The composition of the scale of investigated austenitic stainless steels exposed at high temperature in the presence of chlorides, observed by XRD, is similar, however, the kinetics of corrosion and scale structure varies significantly. Based on the results of the present study schematically shown in Fig. 7 it was found that a higher concentration of Cr and Ni improves the corrosion resistance under the present conditions (steel AISI 310S), whereas a presence of Si further reduces the oxide growth (steels AISI 309 and 314), and its effect is even more pronounced.

Conclusion

Based on the results of tests conducted under atmospheric conditions when alternating between 650°C and room temperature and immersion in an aqueous NaCl solution during the "cold part" of the cycle, the following conclusions can be drawn:

– The corrosion resistance increases in the following way: AISI 321, AISI 304L, AISI 309, AISI 310S and AISI 314.
– The corrosion scale of AISI 304L and AISI 321 is multilayered in cross section and contains various oxides and spinels of alloying elements, the corrosion scale of AISI 309 and AISI 310 contains homogeneous scales containing Fe, Cr and Mn oxides/spinels, while AISI 309 contains a layer with a higher concentration of Ni in addition to the Fe, Cr and Mn oxides/spinels. Regardless the different morphology of the corrosion layers, the XRD analysis of the corrosion products showed no significant difference in the compounds composing the corrosion products of the different tested steel grades.
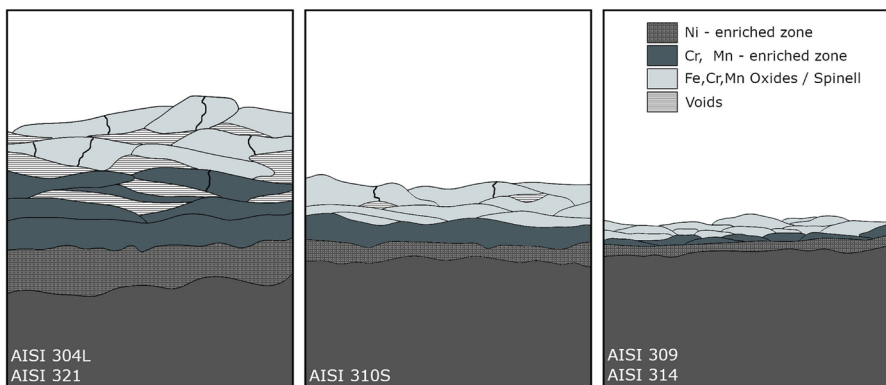
Fig. 7 Scheme of high temperature oxides formed on stainless steels with different amount of Cr, Ni and Si alloying elements

- The chemical composition, i.e. the concentration of Si and of Cr and Ni, plays an important role in the corrosion resistance under the test conditions of this study: the addition of Si at a concentration of 1.8 wt% or more significantly improves the corrosion resistance, regardless of the concentration of Cr and Ni (provided that the concentration of these two elements is high enough for the stainless steel to be austenitic). The simultaneous addition of approximately 5% Cr and 8% Ni is equivalent to addition of approximately 1.5% Si. Si does not form a visible oxide layer but retards the diffusion of Cr and Ni from the alloy into the scale and stabilizes the scale against cracking.
- Under the interface between scale and alloy, there is an enrichment of Ni and a depletion of Cr. This layer is thicker in AISI 304L and AISI 321 than in the other steels tested. Moreover, this layer was found to have a high porosity in steels to which a higher Si concentration was not added (AISI 304L, AISI 321 and AISI 310S).
- According to chemical composition of experimental steels at high-temperature corrosion chromium and iron oxides are formed. Thermodynamically chromium chlorides are preferably formed. According to thermodynamic laws and gained results, simple oxides, such as SiO_2, Cr_2O_3, Fe_2O_3, Fe_3O_4 in FeO and complex oxides, such as $FeCr_2O_4$ and Fe_2SiO_4 are formed.

Declarations

Conflict of interest The authors have no relevant financial or non-financial interests to disclose.

References

1. S. Pedrazzini, E. S. Kiseeva, R. Escoube, et al., *Oxidation Metals* **89**, 2018 (375).
2. G. Mori, K. J. Vidic, E. Bucher, et al., *Materials and Corrosion* **70**, 2019 (1071).
3. Inoue Y, Kikuchi M. Present and Future Trends of Stainless Steel for Automotive Exhaust System. Nippon Steel Technical Report. 2003
4. Lai GY. High-temperature corrosion and materials applications. Materials Park, Ohio: ASM International; 2007.
5. M. Cao, L. Liu, Z. Yu, L. Fan, L. Ying, and F. Wang, *Corrosion Science* **133**, 2018 (165).

6.   HIGH-TEMPERATURE CHARACTERISTICS OF STAINLESS STEEL. Nickel institute; 1979.47.
7.   A. Schmid, G. Mori, E. Bucher, and R. Haubner, *Oxidation Metals* **91**, 2019 (1).
8.   R. Pillai, A. Chyrkin, and W. J. Quadakkers, *Oxidation Metals* **96**, 2021 (385).
9.   H. Fujikawa and N. Maruyama, *Materials Science and Engineering: A.* **120–121**, 1989 (301).
10. C.-J. Wang and C.-C. Li, *Oxidation of Metals* **61**, 2004 (485).
11. F. Wang and Y. Shu, *Oxidation of Metals.* **59**, 2003 (201).
12. Tsaur, Charng-Cheng. High temperature oxidation and NaCl-induced accelerated corrosion of hot-dip aluminized 9Cr-1Mo and 310 stainless steel. Texas A&M University. Texas A&M University: Texas A&M University. Texas A&M University; 2004.127.
13. J. C. Gomez-Vidal and R. Tirawat, *Solar Energy Materials and Solar Cells* **157**, 2016 (234).
14. S. Karlsson, J. Pettersson, L.-G. Johansson, and J.-E. Svensson, *Oxidation Metals* **78**, 2012 (83).
15. Y. Shinata, F. Takahashi, and K. Hashiura, *Materials Science and Engineering* **87**, 1987 (399).
16. Y. S. Li, Y. Niu, and W. T. Wu, *Materials Science and Engineering: A* **345**, 2003 (64).
17. W. M. Lu, T. J. Pan, K. Zhang, and Y. Niu, *Corrosion Science* **50**, 2008 (1900).
18. M. Wang, S. Zeng, H. Zhang, M. Zhu, C. Lei, and B. Li, *High Temperature Materials and Processes* **39**, 2020 (340).
19. M. Sarvghad, G. Will, and T. A. Steinberg, *Solar Energy Materials and Solar Cells* **179**, 2018 (207).
20. R. Pillai, M. Romedenne, J. A. Haynes, and B. A. Pint, *Oxidation Metals* **95**, 2021 (157).
21. P. Sotto Vangeli, B. Ivarsson, and R. Pettersson, *Oxidation Metals* **80**, 2013 (37).
22. D. J. Young and B. Gleeson, *Corrosion Science* **44**, 2002 (345).
23. J. N. Pereira, V. F. de Souza, and A. M. De Sousa Malafaia, *Oxidation Metals* **96**, 2021 (453).
24. L. Mikkelsen, S. Linderoth, and J. B. Bilde-Sørensen, *MSF* **461–464**, 2004 (117).
25. M. H. Davies, M. T. Simnad, and C. E. Birchenall, *JOM* **3**, 1951 (889).
26. H. Buscail, S. E. Messki, F. Riffard, et al., *Materials Chemistry and Physics.* **111**, 2008 (491).
27. H. Buscail, S. El Messki, F. Riffard, S. Perrier, R. Cueff, and C. Issartel, *Journal of Material Science* **43**, 2008 (6960).
28. N. Hiramatsu, Y. Uematsu, T. Tanaka, and M. Kinugasa, *Materials Science and Engineering: A* **120–121**, 1989 (319).
29. V. A. C. Haanappel, T Fransen, and PJ. Gellings, *High Temperature Materials and Processes* **10**, 1992 (67).
30. Y.-N. Chang and F.-I. Wei, *Journal of Material Science* **26**, 1991 (3693).
31. D. J. Young, *High Temperature Oxidation and Corrosion of Metals*, (Elsevier, Amsterdam Oxford Cambridge, 2016).
32. N. Birks, G. H. Meier, and F. S. Pettit, *High-Temperature Oxidation of Metals*, (Cambridge University Press, Cambridge, 2006).
33. J. Pettersson, N. Folkeson, L.-G. Johansson, and J.-E. Svensson, *Oxidation Metals* **76**, 2011 (93).
34. C. Cuevas-Arteaga, J. Uruchurtu-Chavarín, J. González, G. Izquierdo-Montalvo, J. Porcayo-Calderón, and U. Cano-Castillo, *CORROSION.* **60**, 2004 (548).
35. S. C. Okoro, M. Montgomery, F. J. Frandsen, and K. Pantleon, *Oxidation Metals* **89**, 2018 (99).
36. G. Salinas-Solano, J. Porcayo-Calderon, J. G. Gonzalez-Rodriguez, V. M. Salinas-Bravo, J. A. Ascencio-Gutierrez, and L. Martinez-Gomez, *Advances in Materials Science and Engineering* **2014**, 2014 (1).
37. A. A. Tiamiyu, U. Eduok, J. A. Szpunar, and A. G. Odeshi, *Scientific Reports* **9**, 2019 (12116).
38. M. B. Leban and R. Tisu, *Engineering Failure Analysis* **33**, 2013 (430).